A Global Mean Dynamic Ocean Topography

F. Siegismund[1]

[1]Inst. Astr. & Phys.Geodesy, Technische Universität München, Munich, Germany

Key Points:

- The proposed new methodology for land-filling the Mean Sea Surface (MSS) strongly reduces Gibbs effects in the Mean Dynamic Topography (MDT).
- Recent geoid models contain physical information at least up to maximum degree and order (d/o) 420 corresponding to 48km length scale.

Corresponding author: Frank Siegismund, `frank.siegismund@tum.de`

Abstract

The space-born geodetic temporal Mean Dynamic Topography (MDT) is obtained from the difference of altimetric Mean Sea Surface (MSS) h and the geoid height N. With the geostrophic surface currents obtained from its gradient the MDT is an essential parameter when discribing the ocean dynamics. Spectral consistency of h and N is crucial to minimize MDT errors. Usually, h is globalized to allows for a Spherical Harmonic (SH) analysis and small scales beyond maximum degree and order (d/o) resolved in the geoid are cut-off. However, the usual globalization causes ocean-land steps in $h-N$ and spectral inconsistencies of N and h over land. To overcome both issues a new methodology is proposed based on globalization of the MDT. A Laplacian smoother with the coastal MDT values as boundary condition is applied resulting in a flat surface over land and a continuous ocean-land transition. The new methodology strongly reduces Gibbs effects and the need to work with high resolution MDTs to minimize them. Reduction of resolution is tested to reduce MDT uncertainties caused by the commission error expected to increase whith decreasing scale. Applying drifter data and a high resolution hydrodynamic ocean model it is shown, that for the Gulf Stream and the Kuroshio geodetic MDTs applying recent combined geoid models contain physical information up to at least d/o 420 (48km spatial scale). Since for oceanic regions with strong gradients in N still inconsistencies between the geoid and the MSS exist, it depends on application/region if a higher resolution MDT is needed.

1 Introduction

The ocean Dynamic Topography (DT) is a powerful parameter in oceanography. It is defined as the deviation of the geometrical ocean surface from the geoid, which itself is that equipotential surface of gravity closest to the ocean surface in a least-squares sense. Defined like this the geostrophic surface currents follow the isolines of the DT and their strength is determined from the gradient of the DT and the local Coriolis parameter. The geostrophic currents are the equilibrium of horizontal pressure and Coriolis force and quite accurately describe the circulation on large spatial (>1000 km) and temporal (few days and longer) scales.

Applying space-born observations, global maps of the temporal Mean DT (MDT) can be determined as the difference of the temporal mean geometric surface of the ocean h observed from altimetry and the geoid N obtained from gravity measurements. This observation strategy is very powerful providing global maps of a very useful parameter for oceanography that hardly can be obtained by other means. In recent years the U.S./German GRACE (Tapley et al., 2004)), recently extended by its Follow-On, and the ESA GOCE (Rummel et al., 2002) satellite missions have provided high precision gravimetric measurements with respective improvements in the accuracy of gravity-based geoids. Satellite-only geoid models are now available up to degree and order (d/o) 300, corresponding to 67 km spatial resolution. Combined geoid models in addition utilize altimetry data and terrestrial gravity data up to a 5'×5' grid, which corresponds/results in gravity field models and geoids up to approximately d/o 2160.

The computation of the MDT as the difference of h and N, however, is a challenging task since this difference is two orders of magnitde smaller than the two almost identical parameters. In addition, observation strategies and physical nature of the two quantities differ. h is observed as a geometrical quantity and naturally provided on an ocean-only grid, whereas the geoid is a global linear functional of the Earth's gravity potential provided usually in spectral space as Stokes coefficients which result from projecting the potential onto Spherical Harmonic (SH) functions. The small deviation between h and N and comparable or higher spectral power in N compared to the MDT also for small spatial scales makes spectral consistency of N and h a central issue for the quality of the resulting MDT.

The usual strategy for a spectrally consistent combination of h and N to obtain the MDT is the spectral approach as described by Bingham et al. (2008). Here h has to be globalized which needs a filling-in of land values. Then spectral consistency is established by SH analysis, cutting-off the Stokes coefficients for SH functions above maximum d/o n of the applied geoid model and synthesizing back to a desired grid in physical space. Subtraction of N from the globalized and filtered h_n provides the MDT, that is finally spatially filtered if needed.

For the necessary filling-in of land data, usually geoid height from a specific geopotential model is applied. Either the MSS is already provided as global field by the producer and is used unchanged (Sanchez-Reales et al., 2013; Knudsen et al., 2011) or that geoid model is applied which is later also subtracted from the MSS to obtain the MDT (Feng et al., 2013; Sanchez-Reales et al., 2016). Though this filling-in with geoid data is very convenient, it causes two sources of errors when subsequently applying the spectral filter to the globalized MSS:

1. An ocean-land step is inevitable since the MSS is the sum of geoid and MDT while over land only geoid height is set,
2. the geoid data used for land-fill-in is usually spectrally inconsistent with the geoid contained in the MSS over the ocean.

Both issues will cause unphysical wavy noise to spread into the ocean when a spectral cut-off filter is applied. This noise is increasing with decreasing cut-off d/o. The challenges caused by the step in MDT along the coastlines are analysed in Albertella and Rummel (2009). Both issues, the ocean-land step as well as the spectral inconsistency of land and ocean geoid, are tackled in this paper applying an easy to implement approach. The fundamental idea is to understand the MDT as a global field and to define land values as function of the ocean values with the objective to minimize unphysical signals over the ocean when (spectral) filtering is applied. Though it isn't claimed that the objective is fullfilled completely it is shown that the proposed approach solves the dominant ocean-land step problem und by this strongly reduces wavy structures which are common artefacts in low resolution MDT solutions generally caused by small scale information in $h - N$ that is not resolved in the low resolution MDT.

Beside the globalization of h, still following the spectral approach (Bingham et al., 2008), the cut-off maximum d/o of the MDT has to be selected. So far this selection is dominated by the mentioned wavy structure of Gibbs effects caused by the inability to reproduce the ocean-land step with limited spatial resolution, which increases with decreasing maximum d/o and is the dominant error component in low resolution MDTs. Thus high resolution is needed though both the commission error in geoid and MSS is expected to increase with decreasing spatial scale and it isn't known up to which resolution the geodetic MDT actually contains physical information.

With the proposed globalization strategy for h and thereby substantial reduction of noise in low resolution MDT solutions, the trade-off of increasing commission and decreasing omission error with increasing spectral resolution comes into focus when selecting the maximum d/o of the dedicated MDT. To provide useful information about signal content in the small scales of recent geoid models is thus the second subject of this paper. This issue is interesting by itself and will facilitate the appropriate choice of the cut-off d/o in practical applications.

The remaining paper is organized as follows: In section 2 the general methodology to compute an MDT and the applied models for h and N are introduced. For the assessment of surface geostrophic currents obtained from the MDTs we compare with both near-surface drifter data and results from a high-resolution hydrodynamic ocean model of the North Atlantic. Both tools are explained in this section. In section 3 the methodology for globalizing the MSS is introduced. The MDTs and geostrophic surface

currents derived by this approach are assessed by comparison to other commonly used methods. Section 4 is dedicated to small scale signal content in MDTs derived applying recent high-resolution combined geoid models. It is tested to what extend the geostrophic surface currents of the strongest Western boundary currents, the Gulf Stream and the Kuroshio, are reproduced depending on resolution of the MDTs. These currents are selected since here the resolution down to small scales is needed to resolve the full current due to the short across-scale of the currents. In addition, the uncertainty in currents caused by the commission error in both the MSS and the geoid has as low as possible weight due to the large signal strength. In section 5 a conclusion of the main outcomes is provided.

2 Methodology and Approach

2.1 Mean Dynamic Topography

The geodetic MDTs in this paper are computed as deviation of the MSS from the geoid model. Both, MSS and geoid model use the same tide system (tide-free) and reference ellipsoid (TOPEX). The methodology then follows the spectral approach as described in Bingham et al. (2008). In this approach the globalized MSS model is projected to SH functions, cut-off at a specific maximum d/o selected for the MDT and synthesized to a grid the MDT is desired on. Then the geoid is synthesized to the same maximum d/o and grid, and subtracted from the MSS. The resulting MDT is spatially filtered if necessary. For the MSS we apply DTU15 (Andersen et al., 2016). The correction of the land values in this already globalized model is a central subject of this paper and explained and assessed in section 3. The geoid models we apply to compute the different MDTs are listed in Table 1. They are obtained from recent gravity field models available for download at the International Centre for Global Earth Models (ICGEM). For the combined models the newest releases from the different processing centers are chosen. In addition, TIM_R6 (Brockmann et al., 2014) is selected as a recent satellite-only model. The MDTs are computed on a 10'×10' grid. Spatially filtered MDTs are obtained, were needed, by applying a truncated Gaussian kernel with the truncation set at three times the filter length.

The low-resolution geoid model (TIM_R6) is used to compute the MDTs in section 3 applying and comparing different methods for land-filling the MSS. The effects of the proposed new methodology for this task are largest for low resolution MDTs. Therefore and since satellite-only models, specifically including GOCE mission data, have been used frequently in recent years, the TIM_R6 model is used here rather than a high resolution combination model. The GECO model is used to calculate coastal MDT values needed for MSS land-filling with the new methodology explained in Section 3, though the other three very-high-resolution models (SGG-UGM-1, EIGEN6C4, EGM2008) were also tested and show similar results. All combination models are used in section 4 for the investigation of MDT small scale signal content.

With local Cartesian coordinates x and y towards east and north, respectivly, the zonal (meridional) geostrophic surface currents u (v) are calculated from the MDTs as

$$u = -\frac{g}{f}\frac{\partial \zeta}{\partial y} \tag{1}$$

$$v = \frac{g}{f}\frac{\partial \zeta}{\partial x} \tag{2}$$

with g the acceleration due to gravity, ζ the MDT and $f = 2\Omega sin\phi$ the Coriolis parameter, where Ω is the angular speed of the earth and ϕ is the latitude. Practically, the velocities are computed from central MDT differences with u (v) defined on the longitudes (latitudes) of the MDT grid, but on latitudes (longitudes) centered between the two MDT grid points the velocity is computed from. This two-point central difference computation of velocities minimizes smoothing. For practical reasons, the absolute velocity $w =$

Table 1. Gravity field models applied to obtain the geoid height. In the data column, the datasets used in the development of the models are summarized, where S is for satellite (e.g., GRACE, GOCE, Lageos), A is for altimetry, and G for ground data (e.g., terrestrial, shipborne and airborne measurements). If available gravity field models are applied this is also indicated (e.g., GOCO05s, EGM2008).

Model	data	degree	Reference
TIM_R6	S(GOCE)	300	Brockmann et al. (2014)
XGM2016	A,G,S(GOCO05s)	719	Pail et al. (2018)
GOCO05c	A,G,S	720	Fecher et al. (2017)
SGG-UGM-1	EGM2008, S(Goce)	2159	Liang et al. (2018)
GECO	EGM2008, S(Goce)	2190	Gilardoni et al. (2016)
EIGEN6C4	A,G,S(Goce),S(Grace),S(Lageos)	2190	Frst et al. (2014)
EGM2008	A,G,S(GRACE)	2190	Pavlis et al. (2012)

manuscript submitted to *JGR*

$\sqrt{u^2+v^2}$ is defined on the MDT grid applying u and v north and east of the grid point, respectively.

2.2 Geostrophic currents from near-surface drifter data

The drifter data applied in this study is the 6-hourly data set as provided by the Global Drifter Program (GDP, Lumpkin and Pazos (2007)). Only drogue-on drifters are applied (Lumpkin & Johnson, 2013). Available data until December 2014, made up of more than 10 million entries, are used. To estimate the time average surface geostrophic circulation, as can be drawn from the MDT maps, a number of corrections are necessary applying external data wind (NCEP/NCAR reanalysis, Kalnay et al. (1996)) and updated merged Sea Level Anomaly (SLA) provided by the Copernicus Marine Environment Monitoring Service (CMEMS). The methodology generally follows the description in Siegismund (2013), specifically subtracting wind slip of surface buoys, the filtering for inertial currents and subtracting the time variable part of the geostrophic currents calculated from SLA, re-referenced to the period 2002–2013 and linearly interpolated to the drifter positions and time.

However, to secure complete indepedence of drifter data from any MDT used in this study, the estimation of Ekman currents does not use an MDT as reference. Instead, anomalies of the filtered drifter velocities within $5°\times5°$ boxes are calculated. The work of Rio and Hernandez (2003) and Ralph and Niiler (1999) is followed, but instead of the total Ekman current $\vec{U_e}$, the anomaly $\vec{U_e'}$ is estimated as

$$\vec{U_e'} = b(\frac{\vec{\tau}}{\sqrt{f|\tau|}})' e^{i\Theta} \tag{3}$$

with $\tau = c_d * \rho * U_w * |U_w|$ the wind stress, where $c_d = 2.7*10^{-3}*|U_w|^{-1}+1.42*10^{-4}+7.64*10^{-5}*|U_w|$ and $|U_w|$ the wind speed. $'$ stands for the deviation from the mean for the considered box. b and Θ are determined by Least-squares (LS) fitting $\vec{U_e'}$ to the drifter velocity anomalies for each box. No LS fitting is performed for boxes containing not more than 1.000 data points.

All other boxes are checked for unrealistic estimates of b and Θ. Therefor $1ms^{-1}$ westerly wind is supposed and the Ekman current for the box and mean as well as standard deviation of both vector components of the Ekman current for the surrounding 8 boxes are computed. If for at least one vector component the Ekman current of the considered box deviates from the mean of the surrounding boxes by more than 2.5 times the standard deviation, the LS fit is identified as outlier. The check for outliers is iterated for all boxes several times until no outlier is found anymore.

For those boxes with too few drifter data points for the LS fitting or where the results of the fitting are detected as outliers, b and Θ are a function of the parameters in the surrounding boxes, respectively. b is obtained as weighted average. The weighting is set proportional to the reciprocal center-center distance between the boxes. To obtain Θ the Ekman currents for westerly wind are summed but with the lengths of the vectors corrected to the same weighting as used to calculate b. Θ is then set as $\Theta = atan(v_e/u_e)$ with u_e (v_e) the zonal (meridional) component of the vector. For every data point the Ekman currents are calculated and subtracted from the filtered drifter velocities to obtain estimates of temporal mean geostrophic currents at the positions of the filtered drifter velocities.

For the calculation of surface geostrophic velocities across sections as is discussed in Section 4, all velocities from drifters crossing the section are taken into account. The velocity on the section is estimated as the average of the velocity vector before and after the crossing projected to the direction perpendicular to the section. To achieve a substantial averaging-out of errors, from all crossing points all possible 19 neighboring points are grouped. A weighted average of both velocity and position, is computed for each group

applying a reciprocal total velocity weighting (Maximenko, 2004) with the total velocity the sum of geostrophic, Ekman and wind slip component.

RMS differences of drifter and MDT derived geostrophic velocities as discussed in Section 3 are based on evaluations for all drifter velocities in a specified region. The evaluation includes the comparison of the zonal and the meridional velocity component. For the geostrophic velocities derived from the MDT the two components are defined on different grids. The zonal (meridional) component is defined central between two neighbouring MDT grid points on the same longitude (latitude). For a specific drifter data point and component a plane is defined by the three nearest MDT grid points surrounding the drifter data point and the value of that plane for the drifter data point is applied as MDT derived geostrophic velocity component. The (MDT-drifter) difference in surface geostrophic velocity is determined as

$$\Delta w = \sqrt{(\Delta u)^2 + (\Delta v)^2} \tag{4}$$

with Δu (Δv) the difference in the zonal (meridional) velocity component. To obtain spatial mean RMS values not biased by the uneven distribution of the drifter data points, the squared velocity differences are averaged over the boxes of a $1^\circ \times 1^\circ$ grid and then averaged over the region considerd before the square root is applied.

2.3 Hydrodynamic Model

The hydrodynamic model applied is the MIT general circulation model (Marshall et al., 1997) covering the Arctic Ocean and the Atlantic Ocean north of 33°S in a horizontal resolution of 4 km. The model was set up with a bipolar curvilinear grid, with one pole located over North America and the other over Europe. In the vertical, the model setup uses 100 levels of varying depth, from 5 m in the upper ocean to 185 m in the deep ocean. Bottom topography is derived from the ETOPO database in 2' resolution. The model starts from the year 2002 conditions from another model, that has a similar setup with lower resolution of approximately 8 km and itself starts in 1948 from the annual mean temperature and salinity from the World Ocean Atlas 2005 (Boyer et al., 2005). The model simulation spans the period from 2003 to 2009.

The model simulation is forced at the surface by fluxes of momentum, heat, and freshwater computed using bulk formulae and the 6 hourly atmospheric state from the 1989–2009 ECMWF ERA-Interim reanalysis (Dee et al., 2011). At the open southern boundary, the simulations are forced by the output of a 1° resolution global solution of the MITgcm forced by the NCEP data set. A barotropic net inflow of 0.9 Sv (1 Sv $=10^6 m^3 s^{-1}$) into the Arctic is prescribed at Bering Strait, the models' northern open boundary, which balances a corresponding outflow through the southern boundary at 33°S. A dynamic thermodynamic sea ice model solves for sea ice parameters. See Biri et al. (2016) for details.

For the purpose of this study the modeled sea level is saved on a 10'x10' grid applying bilinear interpolation. For regions outside the model grid a Laplacian smoother is applied to obtain a global MDT. The Laplacian smoother solves the Laplacian Equation $\Delta\zeta = 0$ with the MDT values at the margin of the model grid as boundary condition. Different spatial resolutions are realized by successive SH analysis and synthesis steps. Geostrophic currents are obtained with the same method as applied for the geodetic MDTs.

3 Global Mean Dynamic Topography

Geodetic MDTs are derived from the diffence of MSS and geoid height. The spectral inconsistency between the MSS and the geoid is usually solved by filling the land areas of the MSS with geoid information and low-pass filtering the globalized MSS by

performing a SH analysis and cutting off short scales above maximum d/o of the geoid. However, two sources of inconsistency remain after globalizing the MSS that cause unphysical MDT signal when cutting off small scale information in the MSS:

1. a step along the coastline with its height depending on the local amplitude of the MDT,
2. the geoid defined over land misses small scale signal contained in the MSS over the ocean

It is suggested here to globalize the MDT and use high resolution geoid information over land to provide an as best as possible globalization of the MSS which then massively reduces the inconsistency.

3.1 Methodology

Over the ocean the true (error-free) MDT is defined as usual as the difference of true MSS and geoid models, respectively:

$$\zeta(x_o) = h(x_o) - N(x_o) \tag{5}$$

for an arbitrary ocean point x_o. To allow for a globalization that minimizes unphysical signal when cutting-off small scales, a flat continuation from ocean to land is needed. For this, we solve the Laplacian Equation

$$\Delta\zeta(x_l) = 0 \tag{6}$$

for all land points x_l with the coastal MDT values ζ_c as boundary condition. As result, for an arbitrary land point x_l we obtain

$$\zeta(x_l) = g(\zeta_c, x_l) \tag{7}$$

with g the function determined by the Laplace equation.

Though this MDT land definition does not ensure differenciability along the coastlines it at least prevents Gibbs effects caused by the ocean-land step and minimizes small scale land signals that potentially could cause unphysical ocean signals when applying a spectral low-pass filter. Given the true ocean MDT, the unambitious method to fill-in land signals as described above will provide what is here called the 'true' global MDT though better filling approaches might develop with future research. The true global MDT can be projected onto SH functions and expressed as truncated MDT with arbitrary maximum d/o $n > 0$. The necessary succesive SH analysis and synthesis steps are explained in detail e.g. in Bingham et al. (2008).

From the globalization of the MDT, by combining Eqs. 5 and 7, a clear definition for the MSS over land follows:

$$h(x_l) = N(x_l) + \zeta(x_l) = N(x_l) + g(\zeta_c, x_l) \tag{8}$$

for an arbitrary land point x_l. The true global MDT truncated at maximum d/o n can then be descibed as

$$\zeta_n = f_n(h - N) = f_n(h) - f_n(N) \tag{9}$$

where f_n describes the spectral truncation of a globally defined function to maximum d/o n. The error of an MDT, defined up to some maximum d/o n in a real-life application, can be described in terms of the deviation from the 'true' MDT truncated at the same resolution as

$$\begin{aligned} e_{\zeta_n} &= \widetilde{\zeta_n} - \zeta = \widetilde{\zeta_n} - \zeta_n + (\zeta_n - \zeta) = (f_n(\tilde{h}) - f_n(\tilde{N})) - (f_n(h) - f_n(N)) + e_n \\ &= f_n(\tilde{h} - h) - f_n(\tilde{N} - N) + e_n = f_n(e_h) - f_n(e_N) + e_n \end{aligned} \tag{10}$$

with ˜ indicating real-life application fields, e_h the error in the globalized MSS before truncation to the selected maximum d/o and e_N the commisssion error of the geoid model. $e_n = \zeta_n - \zeta$ is the omission error of the MDT caused by missing the signal beyond d/o n. f_n describes the effect of spectrally filtering the errors which causes ringing and other effects depending on spectral distribution of the error and the cut-off d/o.

Since the geoid is usually descibed as a linear functional of SH coefficients, the spectrally filtered error of the geoid $f_n(e_N)$ is a linear function of the SH coefficients up to d/o n and independent of the $h-N$ combination strategy and not discussed here. The omission error e_n is discussed in Section 4.

The MSS error is described as

$$e_h = e_{h_o} + e_{N_l} + e_c \tag{11}$$

and after spectral filtering

$$f_n(e_h) = f_n(e_{h_o}) + f_n(e_{N_l}) + f_n(e_c) \tag{12}$$

e_{h_o} describes the error of the MSS over the ocean and is not discussed here (though MSS at individual points near the coast may be detected as outliers, defined as land points and then are subject to the Laplacian operator, see below). e_{N_l} and e_c are the errors of the geoid model and ζ_c, respectively, applied in Eq. 8 for land filling the MSS.

The suggested strategy to globalize the MSS aims in minimizing both e_{N_l} and e_c. In past applications e_c is usually equal to ζ_c since just a geoid model is already filled-in as MSS land values by the provider or later applied by the user, ignoring the MDT along te coast. The ocean-land step, which is then equal to the coastal MDT values, causes Gibbs effects described in $f_n(e_c)$ when spectrally filtering the MSS. e_{N_l} depends on the geoid model applied. Often, the same geoid model is applied that is later subtracted from $f_n(\tilde{h})$ to compute $\widetilde{\zeta_n}$. If this geoid model comes as a satellite-only model it has low maximum d/o and e_{N_l} contains the missing geoid signal between maximum d/o of the geoid model and maximum d/o of the MSS to be globalized. Spectral filtering of the MSS before combination with the geoid to obtain the MDT will cause a spreading of this error to the ocean and is then seen as error in the MDT.

In our approach we follow Eq. 8 to globalize the MSS. To compute ζ_c we subtract a geoid model from the coastal MSS. The same geoid model is added to the globalized MDT to obtain MSS land values. In general this consistency is not necessary. Also a hydrodynamic model could be applied to derive ζ_c. But any inconsistency of data used left and right of the coastline can cause a step in $\tilde{h} - \tilde{N}$ and is avoided here. The globalized MSS can in general be provided in any resolution m at or above maximum d/o n of the desired MDT and is then spectrally cut as described in Eq. 8. The decision for m will depend on two issues:

1. Since any low-pass filtering is prone to Gibbs-like effects the globalization should be performed as close as possible to the resolution the MSS is originally provided with,
2. geoid information over land has to be available consistent with the chosen resolution m.

Geoid models are nowadays available up to d/o 2160 and it is recommended to use this resolution for the land-filling of the MSS. However, due to limits in available resources maximum d/o will be 1080 here, which is, however, sufficient to show the impact of the approach to the resulting MDT. It is worth noting at this point that the coastal MDT determined to globalize the MSS is not seen as physical signal in the resulting MDT in the end. It is just a mean to compute the 'land MDT' added to the geoid. It is thus not

inconsistent to apply the suggested MSS globalization applying a high resolution combined geoid model and use a satellite-only geoid model to compute the MDT at the end.

The suggested full procedure to compute a global MDT is as follows:

1. A gridded MSS is provided in the spectral resolution of the geoid model applied to compute the MSS land values. We apply DTU15, which is provided on a 1'×1' global grid and apply a spectral analysis/synthesis step to reduce the resolution to maximum d/o 1080 computed on a 10'×10' grid.
2. The geoid chosen for the globalization/correction of the MSS is subtracted to obtain a high resolution MDT ζ_{hf}. We use here different geoid models, see below.
3. The land-sea mask necessary to identify the grid points that need a filling, is provided by the GOCE User Toolbox (GUT), which is also applied for all analysis/synthesis and spatial filtering issues. For outlier detection the geostrophic surface currents based on the ocean points of ζ_{hf} are computed. For both current vector components, if velocity exceeds 3 ms^{-1}, the involved grid points are set to land. This is done to minimize influence of potentially large local MSS errors onto the MDT at some locations near the coast.
4. Based on the coastal values of ζ_{hf} the MDT land values $\zeta(x_l)$ are computed applying the Laplacian equation.
5. $\zeta(x_l)$ is added to the geoid and used as land values for the MSS.
6. The MSS is successively analyzed/synthesized to the spectral resolution n of the resulting MDT.
7. The geoid is computed for maximum d/o n.
8. $\widetilde{\zeta_n} = \widetilde{h_n} - \widetilde{N_n}$
9. MDT land values are set to NaN.
10. A spatial filter is applied, if necessary.

3.2 Impact of MSS correction onto MDT errors

The suggested methodology creating a global MSS is now tested in a practical example. We want to obtain an MDT from DTU15 and the TIM_R6 geoid model. Four approaches to obtain a global MSS are tested:

1. DTU15 is already a global model and is taken as is.
2. TIM_R6 is filled in over land. This is the same model that is subtracted from the MSS to obtain the MDT.
3. Coastal MDT (ζ_c) is computed by subtracting the GECO geoid model truncated at maximum d/o 1080 from the MSS. MSS land values are computed following Eq. 8 applying TIM_R6 for geoid land values $N(x_l)$. This approach minimizes the error e_c along the coastlines but the missing geoid signal between d/o 301 and 1080 is seen in the MSS land error component e_{N_l} (see Eqs. 10–12).
4. Coastal MDT ζ_c is computed as in 3, but the GECO geoid model is applied for land values $N(x_l)$ in Eq. 8. This approach minimizes both e_c and e_{N_l} and is expectedly the best of the four approaches.

The result of the four approaches is displayed in Fig. 1 for the Kuroshio. The first two approaches (upper two rows in Fig. 1), which both include a step in global MDT along the coast line, produce false strong MDT gradients near the coast in some regions and thus unrealistic high surface geostrophic currents. Interestingly, in these approaches the small-scale wavy structure far away from the coast is also more pronounced than in the other two methods. This shows that the way the MSS is globalized is not only important for coastal processes but has also significant offshore effects. If Laplacian smoothing is applied to add a flat MDT signal to the land MSS it remains the choice for the geoid model added to the MDT signal to obtain the MSS over land. If, in our test case,

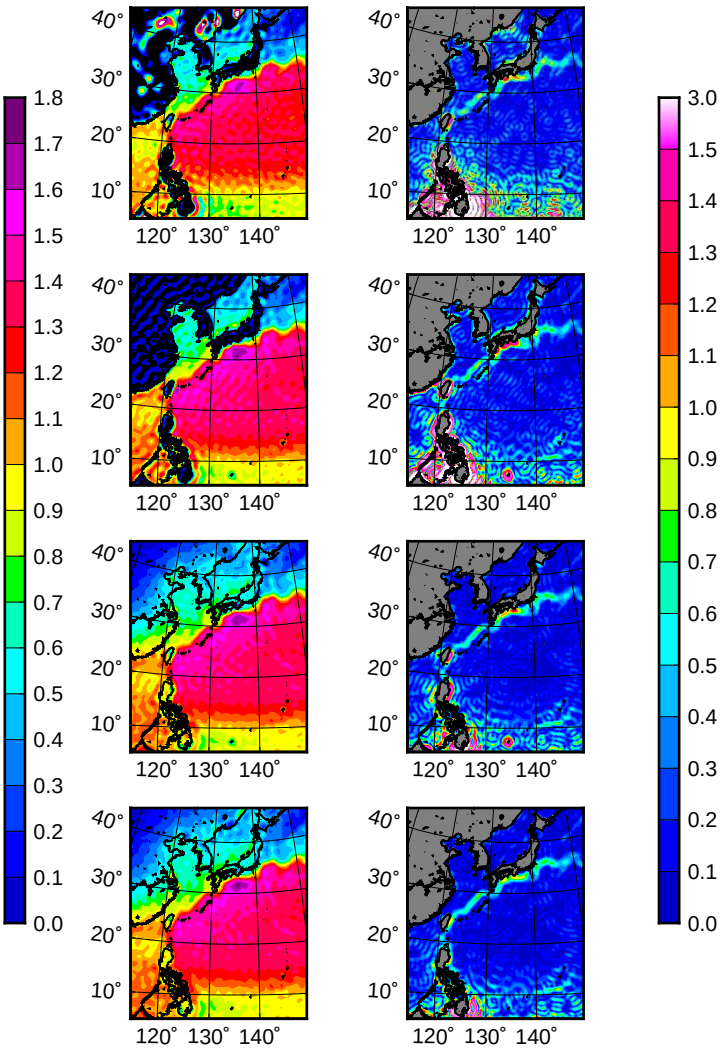

Figure 1. MDT (left, in m) and geostrophic currents (right, in ms^{-1}) as obtained from the four different approaches for land-filling the MSS. Each row refers to one approach in the same order as in the enumerated list in the text.

the low resolution TIM_R6 model is applied (third row in Fig. 1) , still unrealistic high currents result at some individual locations near the coastline, that are not seen when the high resolution GECO model is applied (bottom row in Fig. 1). In summary, spectral inconsistency of the MSS and the geoid model applied for the land fill-in matters regionally. But the land-sea step in MDT is clearly the more important issue when globalizing the MSS with impact on the global ocean. We will thus concentrate in the following onto methodologies 1 and 2, which both include the land-sea step, and approach 4, which we propose here as the best strategy for globalizing the MSS.

For a specific, regional or global application, the choice of the MDT will depend on specific criteria or metrics. As a useful example we apply here the comparison to near-surface drifter data to find the best MDT for two regions (around the Gulf Stream and the Kuroshio, respectively) and the latitudinal band between 60°S and 60°N. Applying DTU15 as MSS and TIM_R6 as geoid model as before, two parameters of the MDT computation recipe as listed in section 3 are varied to find that MDT which fits best the drifter data in the region considered:

1. the maximum d/o of the MDT
2. the length scale of the truncated Gaussian kernel applied as spatial filter

For all regions the cut-off both at maximum d/o 250 and 300 produces rather large RMS values below filter length of 0.6° for all three approaches (Fig. 2) and should not be used. For lower maximum d/o the MDT obtained with approach 4 fits better to the drifter data for all filter lengths and all regions. Specifically for short filter scales and high d/o needed to resolve small scale currents, the RMS for approach 4 is much lower than for the other two aproaches. Quality differences of MDTs from approaches 1 and 2 are not that clear. While globally (60°S-60°N) approach 2 is closer to the drifter data, for the Gulf Stream and the Kuroshio region RMS values for both methods are rather close.

For the Gulf Stream the MDT model following approach 4 with max. d/o 200 and a filter scale of 0.4° fits best to the drifter data. The best model applying a different MSS globalization approach is an MDT with max. d/o 250, 0.6° filter scale and following approach 2. Geostrophic surface currents based on these two MDT models are displayed in the top panels of Fig. 3. It is clearly seen that, though MSS and geoid include small scale information up to d/o 250, due to the stronger spatial filtering necessary when approach 2 is applied, maximum speed in the core of the Gulf Stream is much weaker than for approach 4. Similar results are found for the Kuroshio (bottom panels of Fig. 4), though with somewhat smaller differences in velocities from different approaches. The cut-off maximum d/o is the same as for the Gulf Stream for each of the approaches, respectively while the filter scales are 0.1° longer.

4 Choice of maximum d/o

For the satellite-only geoid model TIM_R6 we applied in the last section we have already seen that it isn't recommended to use this model up to its full resolution of d/o 300. Application of other satellite-only geoid models have revealed similar results (Siegismund, 2013). This might be unevitable due to large commission errors in high d/o SH coefficients, though anisotropic filtering might relax this issue (Bingham, 2010; Cunderlik et al., 2013). With the usual way of globalizing the MSS, Gibbs effects due to small scale land signals and the land-ocean step are unevitable. These effects grow with reducing the spatial resolution of the MDT. Thus, to minimize these effects, a high maximum d/o is needed, no matter if oceanographic signal is included in the small scales. As an example the XGM geoid model is applied to compute (unfiltered) MDTs for maximum d/o 300 to 720 for approaches 1 and 4. Fig. 4 displays the RMS differences of geostrophic surface currents from these MDTs and the corrected near-surface drifter velocities.

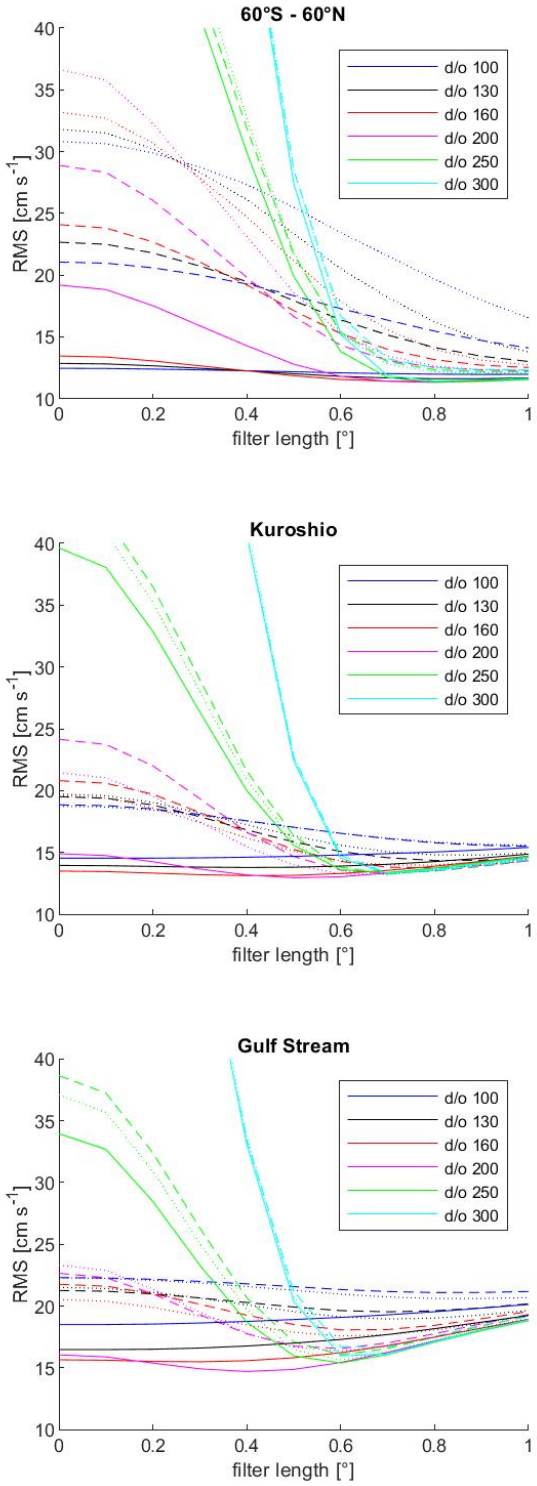

Figure 2. RMS differences $[cms^{-1}]$ of geostrophic surface currents as obtained from geodetic MDTs and corrected near-surface drifter velocities. The MDTs are based on TIM_R6 as geoid models and are computed applying approaches 1, 2 and 4 displayed as dotted, dashed and solid lines, respectively. The three panels show results for (top) the latitudinal band from 60°S–60°S, (middle) the Gulf Stream region (20°–40°N, 85°–60°W) and (bottom) the Kuroshio (20°–40°N, 120°–155°E). For each model and region, MDTs with maximum d/o as listed in the inset and applying a truncated Gaussian filter with filter lengths [0.0°0.1°...1.0°] are tested.

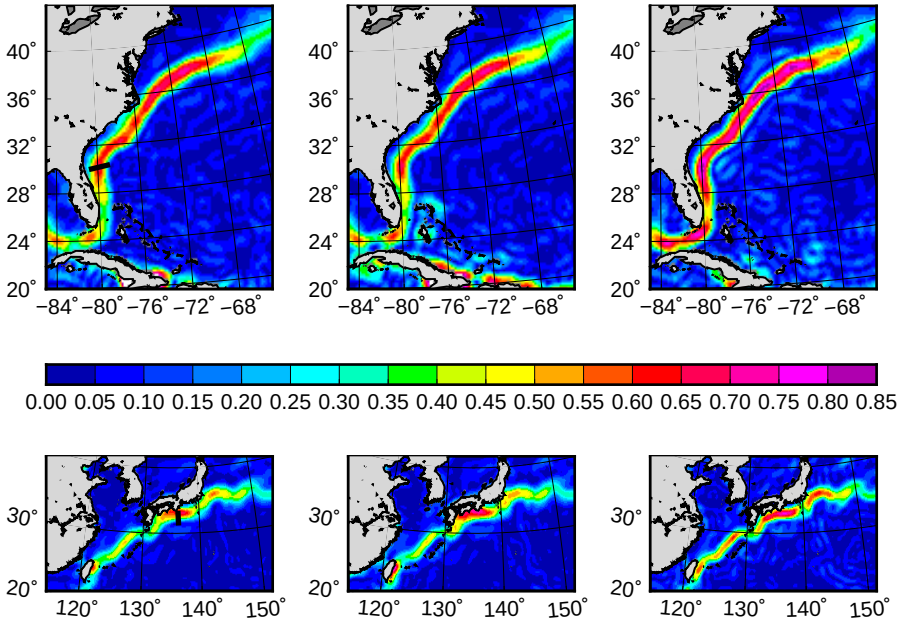

Figure 3. Geostrophic surface velocities [ms^{-1}] from optimized MDT models applying TIM_R6 as geoid model. Optimization is performed for the Gulf Stream region (20°–40°N, 85°–60°W, top panels) and the Kuroshio (20°–40°N, 120°–155°E, bottom panels) by minimizing the RMS difference to corrected near-surface drifter data with respect to different maximum d/o and spatial filter length applied to the MDT. The optimization is done for each of the MSS globalization approaches. For approach 1 (left) and 2 (center) optimal maximum d/o is 250 for both regions, while filter length is 0.6° (0.7°) for the Gulf Stream (Kuroshio). For approach 4 (right) optimal maximum d/o is 200 for both regions and filter length is 0.4° (0.5°) for the Gulf Stream (Kuroshio). Sections crossing the Gulf Stream (top left) and the Kuroshio (bottom left) are plotted as thick black lines. On these sections direct comparisons of drifter and MDT derived geostrophic (near-)surfac currents are performed (see Figs. 5 and 6).

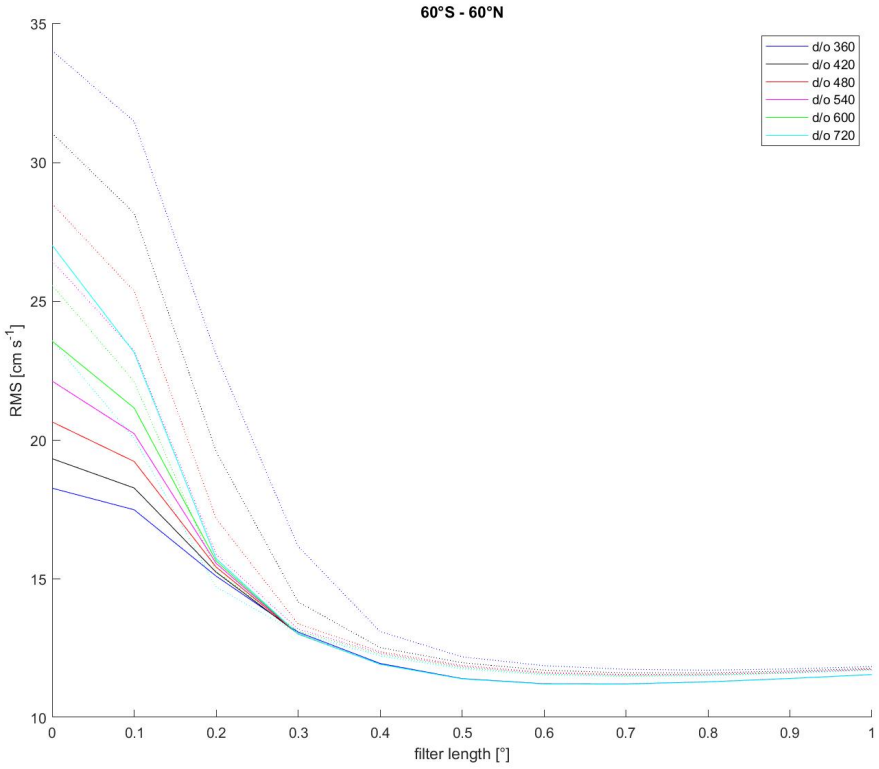

Figure 4. RMS differences $[cms^{-1}]$ of geostrophic surface currents as obtained from geodetic MDTs and corrected near-surface drifter velocities for the latitudinal band between 60S–60N. The MDTs include XGM as geoid model and are computed from approaches 1 and 4 displayed as dotted and solid lines, respectively. For both approaches MDTs with maximum d/o as listed in the caption and applying a truncated Gaussian filter with filter lengths [0.0 0.1 ... 1.] are tested.

It has to be stated that when considering global performance already for maximum d/o 300 the bulk of the MDT signal is resolved since most of the global ocean is covered by large scale gyres rather than small scale currents. Thus, omitted MDT signal is not a dominant source of error. For approach 4 RMS differences are increasing with maximum d/o because of increasing noise in SH coefficients while for approach 1, due to Gibbs effects, the RMS values are much higher and increase with decreasing maximum d/o.

With the Gibbs effects strongly reduced in approach 4 we mainly see the remaining noise in both the geoid model and the MSS and increasing with d/o. Though this noise is an intrinsic part of available MSS and geoid models, sophisticated anisotropic filtering might reduce the issue. But it is asked now up to which maximum d/o signal can be detected in the resulting MDT. With generally growing commission error with higher d/o it might be advisable to cut the MDT beyond this scale to minimize noise without loosing signal.

To address this question, focus is set on the two strongest western boundary currents, the Gulf Stream and the Kuroshio. The short across-current scale needs small-scale information in the MDT to fully resolve the strong gradient in MDT, and the strength of the currents reduces the influence of the commision error as much as possible. For both the Gulf Stream and the Kuroshio one section is selected (see Fig. 3, left panels). The selection is based on the high maximum velocity of the current at this position and the number of available drifter data, respectively.

We compute MDT models applying all six combined geoid models listed in Table 1. For the MDTs that result from subtracting EGM2008, Eigen-6C4, GECO or SGG-UGM-1 from DTU15 the same geoid model is also used to obtain land geoid values for DTU15, while for GOCO05c and XGM the GECO model is applied. Spectral resolution from maximum d/o 100 to d/o 1080 is tested.

For the Gulf Stream the MDT obtained from the hydrodynamic GECCO model is applied for comparison. For this issue the model results are interpolated to a 10'×10' grid, the same that is used for the geodetic MDTs, and the Laplacian smoother is used to fill the grid points outside of the North Atlantic. Then the globalized North Atlantic model is analysed/synthesized to obtain MDTs on the desired maximum d/o.

Currents over a section could be characterized either by absolute speed or the velocity component perpendicular to the section. Errors in the MDT will systematically increase absolute speed assuming independence of the gradients observed in the MDT and in the error, respectively. To prevent potential bias in geostrophic velocities obtained from the geodetic MDTs we consider therefore only the speed perpendicular to the section with random fluctuations caused by errors in the MDT. The accurate orientation of the sections is determined by minimizing along-section speed according to the drifter data.

For all MDT models and both sections up to d/o 420 maximum speed increases with increasing resolution (Figs. 5 and 6). For this resolution maximum velocities have considerable spread between the different MDT models. For the Gulf Stream (Fig. 5) they reach between approximately 75 and 90% of maximum velocity observed in the drifter data. For the Kuroshio (Fig. 6) the geodetic MDTs are very close to the drifter data with the smallest maximum velocities for GOCO05c and Eigen-6c4 reaching around 93% of maximum drifter velocity. Beyond d/o 420 the development is heterogeneous but no model shows substantial increase in maximum velocity. The spatial pattern of the current generally follows quite closely that observed by the drifter data for the Gulf Stream. Only the MDT based on the Eigen-6C4 geoid shows higher currents than all other models 50–100 km offshore the maximum velocity axis. For the Kuroshio the geostrophic currents from the geodetic MDTs do not follow the velocities observed by the drifters so closely. Also, beyond d/o 420 a peak of strong velocity develops close to the point of maximum

velocity as seen by the drifter data and the structure of the current for resolutions beyond max. d/o 720, specifically for max. d/o 1080 is well off the pattern observed by the drifters. For the Gulf Stream the GECCO maximum velocity increases strongly until d/o 480 and reaches max. around d/o 720 close to max. velocity of the drifter data though slightly shifted off-coast.

To get a clearer view on the development of the MDT-derived geostrophic surface currents beyond d/o 420 we map the absolute velocities from all four high resolution geoid models for both the Gulf Stream (Fig. 7) and the Kuroshio (Fig. 8) for max. d/o 420, max. d/o 1080 and the difference (d/o 1080 - d/o 420). From the comparison of the currents itself, for both the Gulf Stream and the Kuroshio, the differences in velocities are hardly detectable. From the mapping of the difference we see for the North Atlantic a structure that seems to follow the Gulf Stream. However, analysing the geoid height we see strong gradients east of the North American east coast and differences in the currents comparing different models beyond d/o 420 seem largely influenced by this effect in the geoid. Much stronger geoid gradients are found in the Northwest Pacific along the margin of the Phillipine Plate. Partly this margin follows closely the path of the Kuroshio and it is not clear whether the differences seen in the currents for different spectral resolution is signal in MDT or resolution-dependent spatial patterns caused by the inconsistency between geoid and MSS in presence of a strong geoid gradient.

5 Conclusions

The computation of geodetic MDTs as difference of MSS and geoid needs spectral consistency of the two fields. Since the geoid is usually derived from Stokes coefficients describing the geopotential field their natural representation is a linear combination of SH functions with cut-off at a specific maximum d/o. To obtain the same representation for the MSS a globalization is needed. This is usually done by filling-in a geoid model over land. This approach, however, causes unphysical wavy structures in the MDT caused by the Gibbs phenomenon from the ocean-land discontinuity in the MSS that reflects the amplitude in coastal MDT, and from spectral inconsistency of the geoid filled in on land and MSS-MDT over the ocean. The new methodology presented in this paper introduces the MDT as a global field with a continuous ocean-land transition and a flat definition over land. To obtain an unambitous global definition the land values of the DT are defined as the solution of the source-free heat equation with the coastal MDT as boundary condition. With this definition any ocean MDT can be globalized and resolution can be reduced via subsequent SH analysis and synthesis. The land values of the MSS are consequently defined as sum of global MDT and geoid model. The coastal MDT values needed to solve the heat equation are obtained from MSS-geoid applying a high resolution geoid model. The same geoid model is then added to the land MDT to obtain the final MSS values.

It is shown that the new methodology reduces strongly the MDT errors near the coast as well as the unphysical waves offshore. Specifically the ocean-land discontinuity from disregarding the coastal MDT with the sofar used MSS globalization causes increasing MDT errors when spectrally reducing resolution. This feature is vanished with the new methodology as is shown by comparison with geostrophically corrected near-surface drifter velocities. Specifically for low maximum d/o the geostrophic velocities from the MDTs fit now much better to the drifter data if the new method is applied. With the old method an as high as possible resolution (with the applied geoid model) was generally necessary to minimize unphysical signals that are caused by both the ocean-land step and ocean/land geoid spectral inconsistency and which grow with decreasing resolution. With this issue strongly diminished, the reduction in spatial resolution is a viable option to reduce the commission error in both geoid and MSS model increasing with spatial frequency.

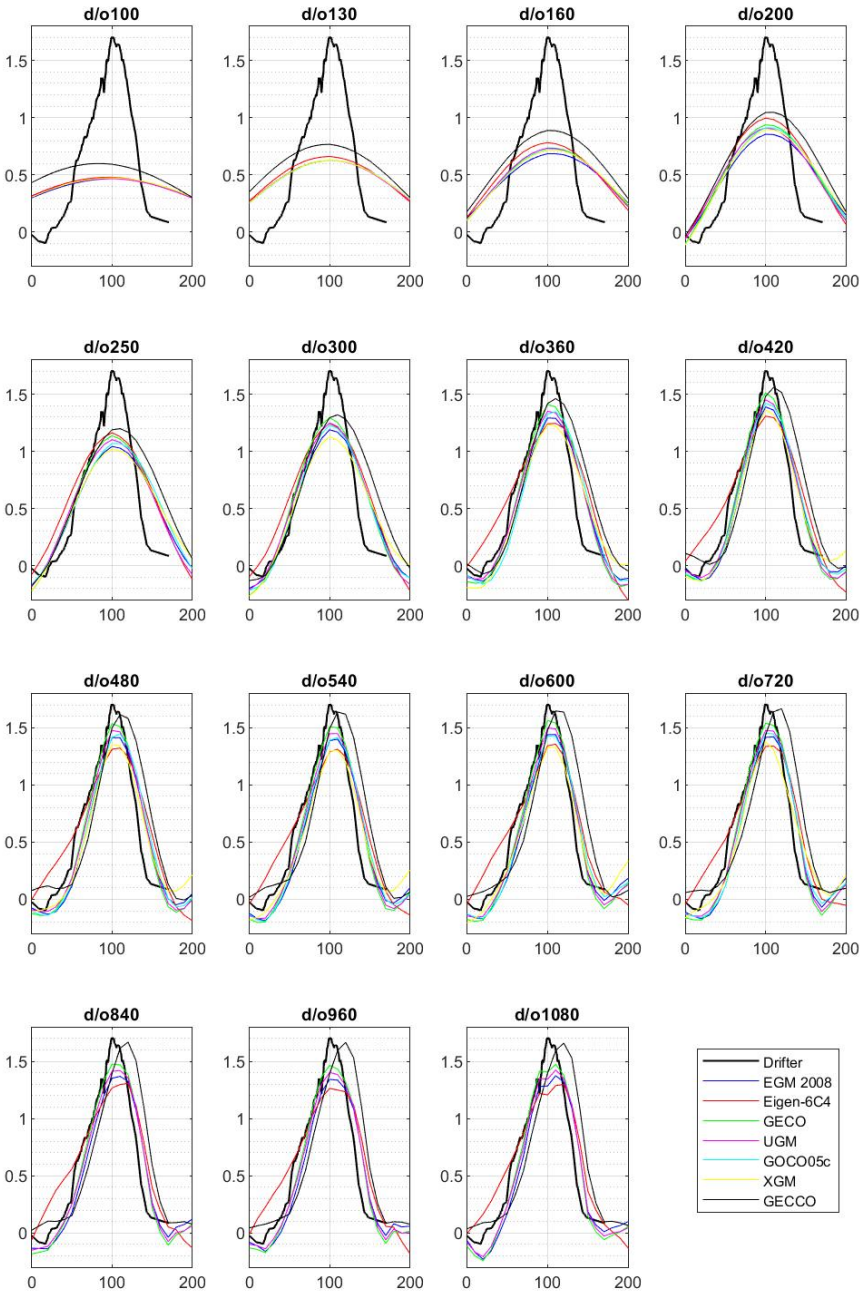

Figure 5. Geostrophic surface velocity [ms^{-1}] over a section across the Gulf Stream (see Fig. 3, top left panel) with the distance over the section provided in [km]. Only the component perpendicular to the section is considered. As listed in the inset, geostrophic surface currents from drifter data and from geodetic and GECCO MDTs are shown. The MDTs are SH analysed/synhtesized for a set of selected resolutions from maximum d/o 100 to 1080 each resolution shown in a separate panel.

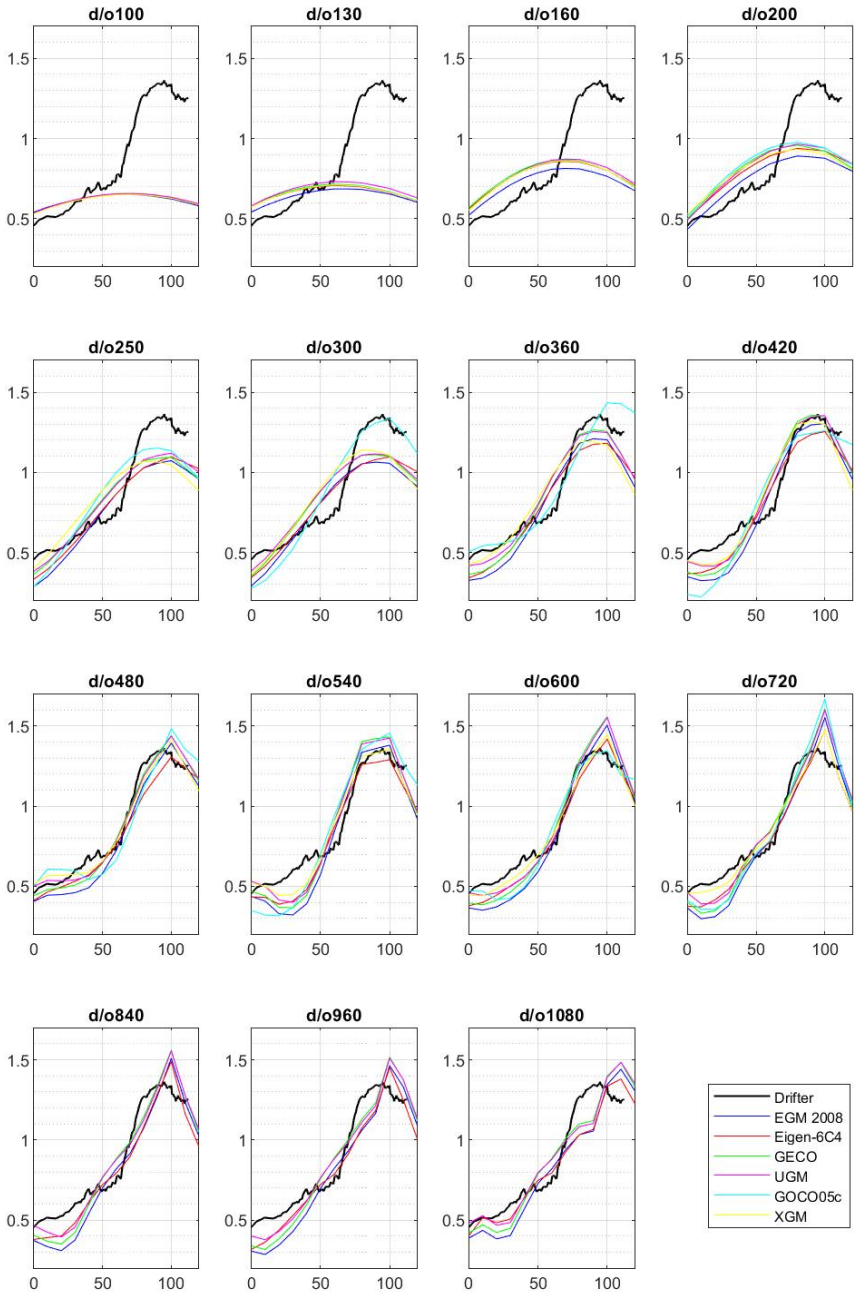

Figure 6. Same as Fig. 5, but for a section over the Kuroshio (see Fig. 3, bottom left panel).

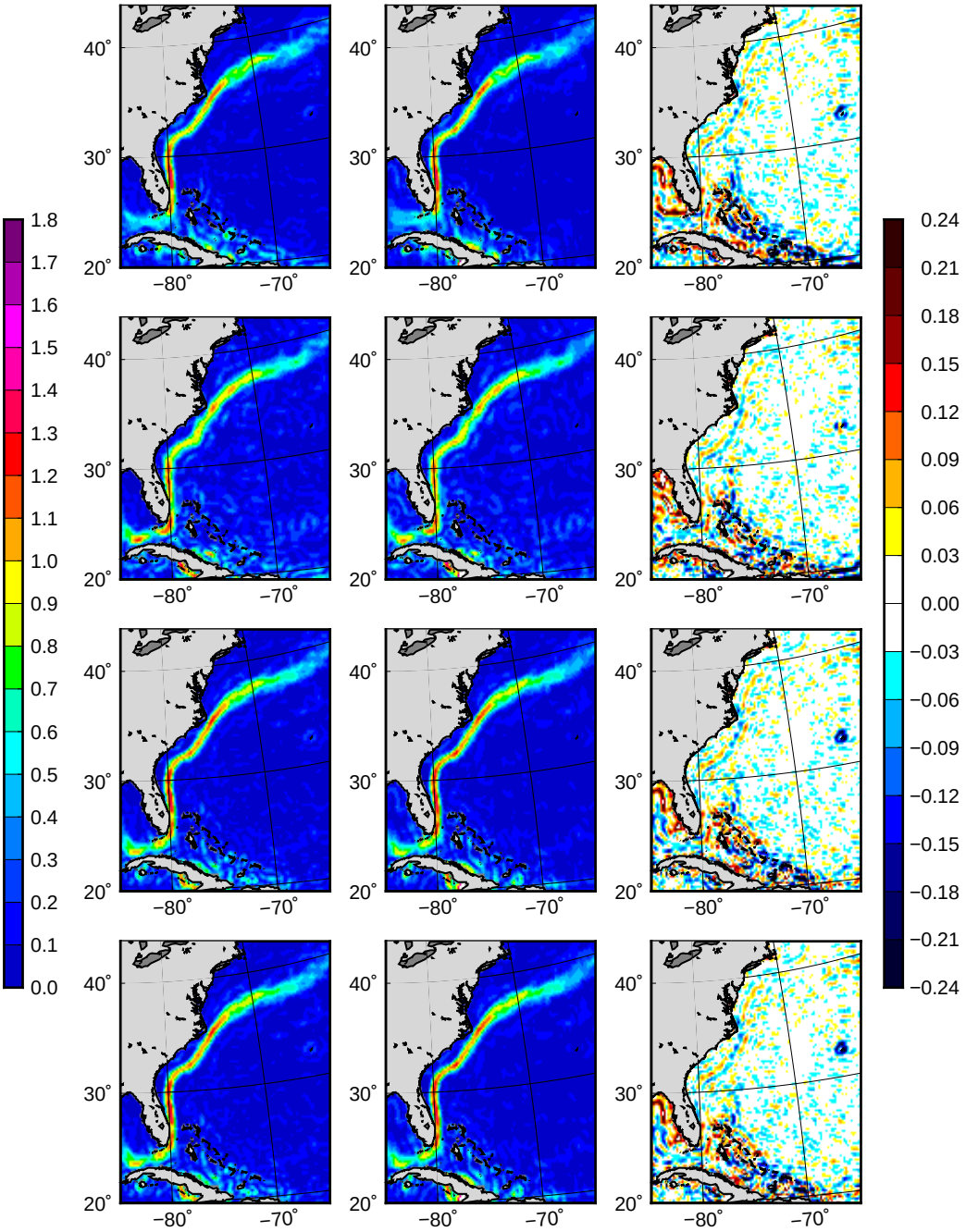

Figure 7. Absolute geostrophic surface currents $[ms^{-1}]$ for the Gulf Stream region from geodetic MDTs applying (from top to bottom) EGM2008, Eigen6C4, GECO and SGG-UGM-1 as geoid models for (left) maximum d/o 420, (middle) d/o 1080 and (right) the difference (d/o 1080-d/o 420). All MDT models are spatially filtered applying a truncated Gaussian kernel with 0.2 filter length.

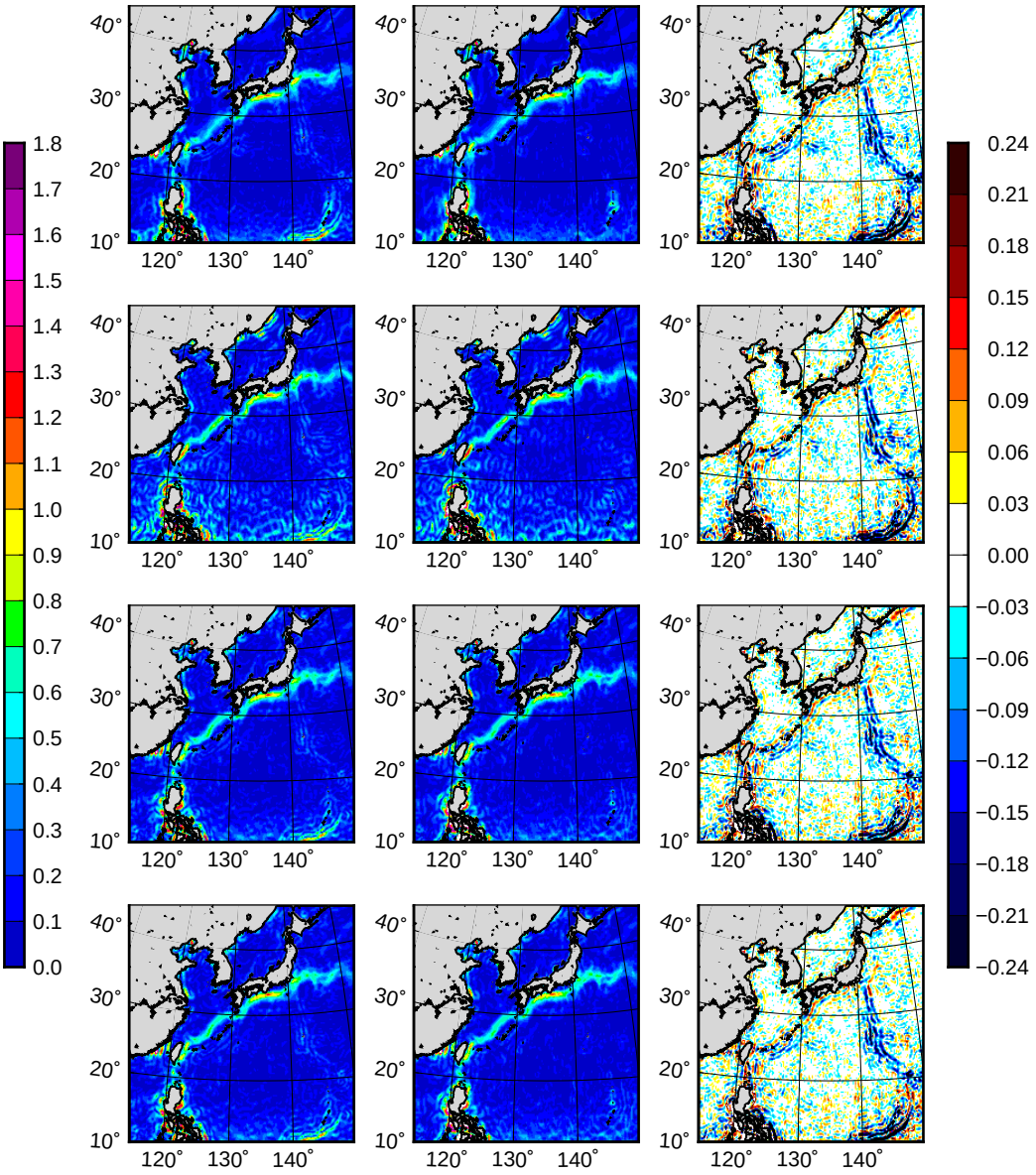

Figure 8. Same as Fig. 7, but for the Kuroshio.

To provide assistance for the choice of the MDT spatial resolution in practical applications, and as an interesting issue by itself, it is tested up to which maximum d/o physical signal is detectable in MDTs applying recent geoid models and DTU15 as MSS model. For two sections, one over the Gulf Stream and another one over the Kuroshio the reconstruction of surface geostrophic velocities is investigated by comparison to drifter data and results of a high resolution dynamic ocean model. Different resolutions up to maximum d/o 1080 are tested. Specifically, increasing maximum velocity over the section is supposed as indicator that small scale information is added when resolution is increased. It is shown that all MDT models show increasing signal up to d/o 420 for both sections. Above this resolution, however, the evolution with increasing resolution is not clear. Strong geoid gradients exist close to both currents. Inconsistencies of MSS and geoid model seem to cause wavy structures that interfere with the currents generating spatial patterns depending on resolution. Further investigation is needed.

Acknowledgments

The sea level anomaly data used in this paper is provided by the Copernicus Marine Environment Monitoring Service (CMEMS). Computations needed to obtain geodetic MDTs were performed applying the GOCE User Toolbox (GUT) provided by the European Space Agency (ESA) and available at https://earth.esa.int/web/guest/software-tools/gut/about-gut/overview. Support of the research was provided by the ESA funded project GOCE-OGMOC (Contract Change Notice No. 9 to Contract No. 18308/04/NL/MM).

References

Albertella, A., & Rummel, R. (2009). On the spectral consistency of the altimetric ocean and geoid surface: a one-dimensional example. *Journal of Geodesy*, *83*(9), 805–815. (doi: 10.1007/s00190-008-0299-5)

Andersen, O. B., Stenseng, L., Piccioni, G., & Knudsen, P. (2016). The dtu15 mss (mean sea surface) and dtu15lat (lowest astronomical tide) reference surface. In *Esa living planet symposium 2016, prague, czech republic.*

Bingham, R. (2010). *Remote Sensing Letters*, *1:4*, 205–212. (doi:10.1080/01431161003743165)

Bingham, R., Haines, K., & Hughes, C. W. (2008). Calculating the ocean's mean dynamic topography from a mean sea surface and a geoid. *Journal of Atmospheric and Oceanic Technology*, *25*(10), 1808–1822. (doi: 10.1175/2008JTECHO568.1)

Biri, S., Serra, N., Scharffenberg, M. G., & Stammer, D. (2016). Atlantic sea surface height and velocity spectra inferred from satellite altimetry and a hierarchy of numerical simulations. *J. Geophys. Res. Oceans*, *121*, 4157–4177. doi: 10.1002/2015JC011503

Boyer, T. P., Levitus, S., Garcia, H., Locarnini, R., Stephens, C., & Antonov, J. (2005). Objective analyses of annual, seasonal, and monthly temperature and salinity for the world ocean on a 0.25 grid. *Int. J. Climatol.*, *25*(7), 931–945.

Brockmann, J. M., Zehentner, N., Hock, E., Pail, R., Loth, I., Mayer-Gurr, T., & Schuh, W. D. (2014). Egm_tim_rl05: An independent geoid with centimeter accuracy purely based on the goce mission. *Geophysical Research Letters*, *41*(22), 8089-8099. doi: 10.1002/2014gl061904

Cunderlik, R., Mikula, K., & Tunega, M. (2013). Nonlinear diffusion filtering of data on the earth's surface. *J. Geod.*, *87*, 143–160. (doi: 10.1007/s00190-012-0587-y)

Dee, D. P., et al. (2011). The era-interim reanalysis: configuration and performance of the data assimilation system. *Quarterly Journal of the Royal Meteorological Society*, *137*(656), 553-597. doi: 10.1002/qj.828

Fecher, T., Pail, R., Gruber, T., & the GOCO consortium. (2017). Goco05c: A new combined gravity field model based on full normal equations and regionally varying weighting. *Surveys in Geophysics*, *38*(3), 571–590.

Feng, G., Jin, S., & Sanchez-Reales, J. M. (2013). Antarctic circumpolar current from satellite gravimetric models itg-grace2010, goce-tim3 and satellite altimetry. *Journal of Geodynamics*, *72*, 72–80.

Frst, C., Bruinsma, S. L., Abrikosov, O., Lemoine, J.-M., Marty, J. C., Flechtner, F., ... Biancale, R. (2014). *Eigen-6c4 the latest combined global gravity field model including goce data up to degree and order 2190 of gfz potsdam and grgs toulouse* (Tech. Rep.). GFZ German Research Centre for Geosciences. (doi: 10.5880/ICGEM.2015.1)

Gilardoni, M., Reguzzoni, M., & Sampietro, D. (2016). Geco: a global gravity model by locally combining goce data and egm2008. *Studia Geophysica et Geodaetica*, *60*, 228–247. doi: 10.1007/s11200-015-1114-4

Kalnay, et al. (1996). The ncep/ncar 40-year reanalysis project. *Bull. Amer. Meteor. Soc.*, *77*, 437–470.

Knudsen, P., Bingham, R., Andersen, O., & Rio, M. H. (2011). A global mean dynamic topography and ocean circulation estimation using a preliminary goce gravity model. *Journal of Geodesy*, *85*, 861–879. (doi: 10.1007/s00190-011-0485-8)

Liang, W., Xu, X., Li, J., & Zhu, G. (2018). The determination of an ultra high gravity field model sgg-ugm-1 by combining egm2008 gravity anomaly and goce observation data. *Acta Geodaeticaet Cartographica Sinica*, *47*(4), 425–434. doi: 10.11947/j.AGCS.2018.20170269

Lumpkin, R., & Johnson, G. C. (2013). Global ocean surface velocities from drifters: Mean, variance, el niño-southern oscillation response, and seasonal cycle. *Journal of Geophysical Research: Oceans*, *118*, 2992–3006. doi: 10.1002/jgrc.20210

Lumpkin, R., & Pazos, M. C. (2007). Measuring surface currents with surface velocity program drifters: The instrument, its data, and some recent results. In *Lagrangian analysis and prediction of coastal and ocean dynamics* (pp. 39–67). Cambridge University Press.

Marshall, J., Hill, C., Perelman, L., & Adcroft, A. (1997). Hydrostatic, quasi-hydrostatic and nonhydrostatic ocean modelling. *J. Geophys. Res.*, *102*, 5733-5752.

Maximenko, N. (2004). Correspondence between lagrangian and eulerian velocity statistics at the asuka line. *J. Oceanography*, *60*, 681–687.

Pail, R., Fecher, T., Barnes, D., Factor, J. F., Holmes, S. A., Gruber, T., & Zingerle, P. (2018). Short note: the experimental geopotential model xgm2016. *Journal of Geodesy*, *92*(4), 443–451.

Pavlis, N. K., Holmes, S. A., Kenyon, S. C., & Factor, J. K. (2012). The development and evaluation of the earth gravitationalmodel 2008 (egm2008). *Journal of Geophysical Research*, *117*. (B04406) doi: 10.1029/2011JB008916

Ralph, E. A., & Niiler, P. (1999). Wind-driven currents in the tropical pacific. *Journal of Physical Oceanography*, *29*, 2121–2129.

Rio, M.-H., & Hernandez, F. (2003). High-frequency response of wind-driven currents measured by drifting buoys and altimetry over the world ocean. *Journal of Geophysical Research*, *108*(C8). doi: 10.1029/2002JC001655

Rummel, R., Balmino, G., Johannessen, J., Visser, P., & Woodworth, P. (2002). Dedicated gravity field missions - principles and aims. *Journal of Geodynamics*, *33*(1–2), 3–20.

Sanchez-Reales, J. M., Andersen, O. B., & Vig, M. I. (2016). Improving surface geostrophic current from a goce-derived mean dynamic topography using edge-enhancing diffusion filtering. *Pure Appl. Geophys.*, *173*, 871–884. (doi 10.1007/s00024-015-1050-9)

Sanchez-Reales, J. M., Vigo, M. I., Jin, S., & Chao, B. (2013). Global surface geostrophic ocean currents derived from satellite altimetry and goce geoid. *Marine Geodesy*, *35*(S1), 175–189. (doi: 10.1080/01490419.2012.718696)

Siegismund, F. (2013). Assessment of optimally filtered recent geodetic mean dynamic topographies. *Journal of Geophysical Research: Oceans*, *118*, 108–117. doi: 10.1029/2012JC008149

Tapley, B. D., Bettadpur, S., Watkins, M. M., & Reigber, C. (2004). The gravity recovery and climate experiment: mission overview and early results. *Geophys. Res. Lett.*, *31*. (L09607 , doi:10.1029/2004GL019920)